Science Bulletin 64 (2019) 1207–1214

Contents lists available at ScienceDirect

Science Bulletin

journal homepage: www.elsevier.com/locate/scib

Science Bulletin
www.scibull.com

Article

Topological vortex phase transitions in iron-based superconductors

Shengshan Qin [a,b], Lunhui Hu [c,a], Xianxin Wu [d], Xia Dai [b], Chen Fang [b,a,e], Fu-Chun Zhang [a,e,*], Jiangping Hu [b,a,e,f,*]

[a] Kavli Institute of Theoretical Sciences, University of Chinese Academy of Sciences, Beijing 100049, China
[b] Beijing National Research Center for Condensed Matter Physics, and Institute of Physics, Chinese Academy of Sciences, Beijing 100190, China
[c] Department of Physics, University of California, San Diego, CA 92093, USA
[d] Institute for Theoretical Physics and Astrophysics, Julius-Maximilians University of Würzburg, Am Hubland, D-97074 Würzburg, Germany
[e] CAS Center for Excellence in Topological Quantum Computation, University of Chinese Academy of Sciences, Beijing 100049, China
[f] Collaborative Innovation Center of Quantum Matter, Beijing 100049, China

ARTICLE INFO

Article history:
Received 25 February 2019
Received in revised form 4 June 2019
Accepted 8 July 2019
Available online 15 July 2019

Keywords:
Weak topological insulators
Vortex bound states
Majorana modes
Iron-based superconductors

ABSTRACT

We study topological vortex phases in iron-based superconductors. Besides the previously known vortex end Majorana zero modes (MZMs) phase stemming from the existence of a three dimensional (3D) strong topological insulator state, we show that there is another topologically nontrivial phase as iron-based superconductors can be doped superconducting 3D weak topological insulators (WTIs). The vortex bound states in a superconducting 3D WTI exhibit two different types of quantum states, a robust nodal superconducting phase with pairs of bulk MZMs and a full-gap topologically nontrivial superconducting phase which has single vortex end MZM in a certain range of doping level. Moreover, we predict and summarize various topological phases in iron-based superconductors, and find that carrier doping and interlayer coupling can drive systems to have phase transitions between these different topological phases.

1. Introduction

For the possible application in quantum computation, the search for Majorana zero modes (MZMs) has been one of the most intriguing topics in condensed matter physics [1]. MZMs usually arise as $(d-1)$-dimensional edge modes of d-dimensional topological superconductors [2–5] (TSCs), and the classification for TSCs has been thoroughly analyzed for different symmetry classes in different dimensions [6,7]. In recent years, many theories have been proposed to realize MZMs [8–28] and signatures for the existence of MZMs in superconductors (SCs) have also been observed in experiments [29–38]. 1D p-wave spinless SCs and 2D $p+ip$-wave SCs are examples of TSCs [1–5,8]. However, the existence of p-wave or $p+ip$-wave SCs has not been experimentally confirmed without a doubt. The discovery of topological insulators [39–42] (TIs) is a breakthrough in the pursuit for TSCs. It is found that, the topologically protected surface Dirac cone of a 3D strong topological insulator (STI) combined with s-wave superconductivity, is equivalent to a $p+ip$-wave spinless SC [9]. As a result, a single MZM can be trapped in a vortex in such a system. Soon after, Hosur et al. [43] introduce the concept of vortex phase transitions (VPTs), and point out that if a STI can be doped to be bulk superconducting, there can also be a single MZM at the vortex core on its surface. Based on the concept of VPTs, a recent work points out that a 1D robust gapless phase with pairs of bulk MZMs, can be realized in doped superconducting topological Dirac semimetals (TDSs) [44]. Besides the well-known candidates for the STIs and TDSs [45–48], there is another interesting class of topological systems, the weak topological insulators (WTIs) [5,49], which can be viewed as 2D TIs sticked together weakly in the third direction. However, there are very few candidates for 3D WTIs. The study of the VPTs in a superconducting 3D WTI has not been carried out.

Recently, the topological properties in iron-based SCs predicted theoretically [50–52] have gained a major support by new experimental evidence [37,38] in $FeSe_{1-x}Te_x$. It is possible that iron-based SCs can be unique promising systems to realize MZM at much higher temperature. The MZMs arise in the vortices in $FeSe_{1-x}Te_x$ because there is an intrinsic band inversion at the Z point. The band inverson leads to a 3D STI state with topologically protected surface states. Following the Fu-Kane proposal [9], the vortex in the superconducting surface states naturally hosts an MZM phase. However, iron-based superconductors are known to be versatile for their structures. In particular, the electronic structure and layer coupling along c-axis can be varied significantly. For example, a zero bias peak is also observed in another iron-based SC,

* Corresponding authors.
E-mail addresses: fuchun@ucas.ac.cn (F.-C. Zhang), jphu@iphy.ac.cn (J. Hu).

https://doi.org/10.1016/j.scib.2019.07.011
2095-9273/

$(Li_{0.84}Fe_{0.16})$OHFeSe [53], whose electronic structure differs significally from $FeSe_{1-x}Te_x$ in three major ways: (1) the former is with much heavier electron doping than the latter; (2) the former has no hole pocket at the Γ point; (3) the coupling between FeSe layers is much weaker in the former than in the latter. These differences question whether $(Li_{0.84}Fe_{0.16})$OHFeSe can be treated as a 3D STI.

In this paper, we show that there are two additional VPTs in iron-based SCs as superconducting 3D WTI. First, for the VPTs in a superconducting 3D WTI with both time reversal symmetry (TRS) and inversion symmetry, we derive the following essential results. Depending on crystalline symmetries and orbitals contributing to the band inversions, the superconducting 3D WTI with a single quantum vortex line can be classified into two cases: (1) if the band inversions occur on a C_n $(n > 2)$ rotational axis and the angular momenta of the orbitals contributing to the band inversions are not equivalent, the superconducting vortex line has a robust nodal phase with pairs of bulk MZMs; otherwise (2) the vortex line is fully gapped and there exist vortex end MZMs in a certain range of doping level. In both cases, the topological phase transition can take place by tuning chemical potentials or Fermi levels. The range of the chemical potential corresponding to the topologically nontrivial phase is proportional to the band dispersion along the weak coupling direction. We also extend our conclusions to a class of normal insulators. Second, we show that the above theory can be applied to classify the topological vortex phases and understand recent experimental results on iron-based SCs. Both band inversions at the Γ and M points in the band strucure of iron-based SCs can generate topological VPTs. For example, the nodal superconducting vortex line phase can be realized by further electron doping in FeSe/Te and LiFeAs [54]. For $(Li_{1-x}Fe_x)$OHFeSe, different topological vortex phases can be realized by changing x. It is also possible that the vortex end MZMs on the (001) surface $(Li_{0.84}Fe_{0.16})$OHFeSe can stem from the 3DWTI state caused by the band inversion at M points discussed in Ref. [50].

2. General theory for 3D WTIs

We consider a general spinful system with intrinsic s-wave spin-singlet superconductivity. The superconducting Hamiltonian in the basis $\Psi^\dagger(\mathbf{k}) = (c_\uparrow^\dagger(\mathbf{k}), c_\downarrow^\dagger(\mathbf{k}), c_\uparrow(-\mathbf{k}), c_\downarrow(-\mathbf{k}))$ can be written as

$$H_{sc} = \begin{pmatrix} H_0(\mathbf{k}) - \mu & \Delta \\ \Delta^\dagger & \mu - H_0^*(-\mathbf{k}) \end{pmatrix}, \tag{1}$$

where we have only preserved the indices for the spin and Nambu spaces. Here, Δ is the superconducting order parameter and takes the form $\Delta_0 i\sigma_2$ in the spin space, μ is the chemical potential, and $H_0(\mathbf{k})$ is the normal state Hamiltonian. If a single quantum vortex goes through the system along the z-direction, the superconducting order parameter $\Delta(\mathbf{r})$ in the real space is transformed into $\Delta(r)e^{i\theta}$, where $r = \sqrt{x^2 + y^2}$ and θ is the polar angle [43,55]. Obviously, the vortex line destroys the translational symmetry in the xy-plane. The TRS is broken while the particle-hole symmetry is preserved. Consequently, such a spinful superconducting system with a single quantum vortex line belongs to the class D of the Altland-Zirnbauer classification [6,7].

We first analyze the topological phase of such a superconducting vortex line by assuming that it is a full-gap system. For a full-gap class D system, it has a Z_2 topological classification. The topological invariance is defined as

$$\nu = \mathrm{sgn}(Pf(H_{sc}(k_z = 0)) \cdot Pf(H_{sc}(k_z = \pi))), \tag{2}$$

where sgn() is the signum and $Pf()$ is the Pfaffian of a antisymmetric matrix [6,7,56]. In the following, we take $Pf(k_z)$ for $Pf(H_{sc}(k_z))$ for simplicity. From Eq. (2), the topological VPTs of such a system are merely determined by the gap close-and-reopen processes at $k_z = 0$ $(k_z = \pi)$. Moreover, it has been concluded that [44], in a superconducting 2D TI if the Fermi energy is in the insulating gap, there is a correspondence between its helical edge modes and the fermion parity of the corresponding vortex bound states: in the normal state, a π-flux always pumps one electron across the Fermi energy (the fermion parity of the system changes from even to odd); if a weak superconducting order is turned on, the fermion parity of the whole system remains unchanged. Thus, if the normal state Hamiltonian describes a 2D insulator in the $k_z = 0$ $(k_z = \pi)$ plane, $\mathrm{sgn}(Pf(0))$ $(\mathrm{sgn}(Pf(\pi)))$ is simply given by the Z_2 topological invariance of the 2D insulator in the $k_z = 0$ $(k_z = \pi)$ plane, and if it is a TI in the $k_z = 0$ $(k_z = \pi)$ plane, $\mathrm{sgn}(Pf(0))$ $(\mathrm{sgn}(Pf(\pi)))$ must change sign at some critical chemical potential $\mu_c(0)$ $(\mu_c(\pi))$.

For a superconducting WTI, if the vortex line is along the weak coupling direction, assuming that the system is full-gap, we can conclude that the superconducting vortex line is topologically trivial if the chemical potential is in the insulating gap of the normal state, and that the vortex line is nontrivial if the chemical potential is between $\mu_c(0)$ and $\mu_c(\pi)$. In the latter case, there are vortex end MZMs even though there exist no topologically nontrivial surface states.

To be specific, we consider a lattice model

$$\begin{aligned} H_0^{(1)} = {} & (m - t\cos k_x - t\cos k_y - t_3\cos k_z)\Sigma_{30} + t'\sin k_x\Sigma_{11} \\ & + t'\sin k_y\Sigma_{12} + t_3'\sin k_z\Sigma_{13}, \end{aligned} \tag{3}$$

in which $\Sigma_{ij} = \tau_i\sigma_j$, and the parameters are taken as $\{t, t_3, t', t_3'\} = \{1.0, 0.5, 1.0, 1.0\}$. Here, τ_i and σ_i $(i = 0, 1, 2, 3)$ are Pauli matrices representing the orbital and spin degrees of freedom. This model respects the TRS and the full symmetry of the D_{4h} point group. The related symmetry group generators are given by the following matrices: $I = \Sigma_{30}, C_{4z} = \tau_0 \otimes e^{i\sigma_z\pi/4}, C_{2x} = \tau_0 \otimes e^{i\sigma_x\pi/2}$ and $T = i\Sigma_{02}K$, where K is the complex conjugate operation. Obviously, the basis of the above model contains two Kramers' doublets with opposite parity, and each Kramers' doublet have angular momentum $\pm\frac{1}{2}$. In the calculations, we set $m = 1.2$ to derive a WTI. With these parameters, $H_0^{(1)}$ has two band inversions at the Γ point and Z point, and it has no topologically nontrivial surface states on the (001) surface while there are two Dirac cones on the (100) surface.

Assuming on-site intra-orbital pairing, we analyze the topological VPTs in the WTI depicted by $H_0^{(1)}$ numerically. In the calculations, we take a simple form of $\Delta(r) : \Delta(r) = \Delta_0\Theta(r - R)$, where $\Theta(r)$ is the step function and R is the vortex size. By diagonalizing the Hamiltonian, we obtain the energy spectrum in the superconducting vortex line. It turns out that the vortex line is indeed fully gapped. If we tune the chemical potential continuously, the energy spectrum of the system becomes gapless at $\mu_1^c = 1.14$ $(\mu_2^c = 0.716)$ at $k_z = 0$ $(k_z = \pi)$, shown in Fig. 1a and b, indicating that the system goes through two topological VPTs. By calculating the Z_2 topological index directly, we find that a topological phase transition occurs when $\mu_1^c = 1.15$ $(\mu_2^c = 0.7)$ at $k_z = 0$ $(k_z = \pi)$, and the system is topologically nontrivial when $\mu_2^c < \mu < \mu_1^c$, as shown in Fig. 1c. The results of the two different methods are consistent. In the topologically nontrivial phase, there must be vortex end MZMs on the (001) surface. To show this, we calculate the local density of states near the vortex core on the (001) surface. Fig. 1d shows the result for $\mu = 1.0$. Obviously, there is a zero-bias peak at the vortex core. Moreover, the zero-bias peak is contributed by different spin components unequally, which leads to spin polarized zero-bias conductance peak in scanning tunneling microscope (STM) experiment [57–59].

It is worth to mention that, the topological VPTs in the superconducting WTI can also be determined by the Berry phase framework in Ref. [43]: the VPT point corresponds to such a condition that the eigenvalues of the $SU(2)$ Berry connection on the Fermi

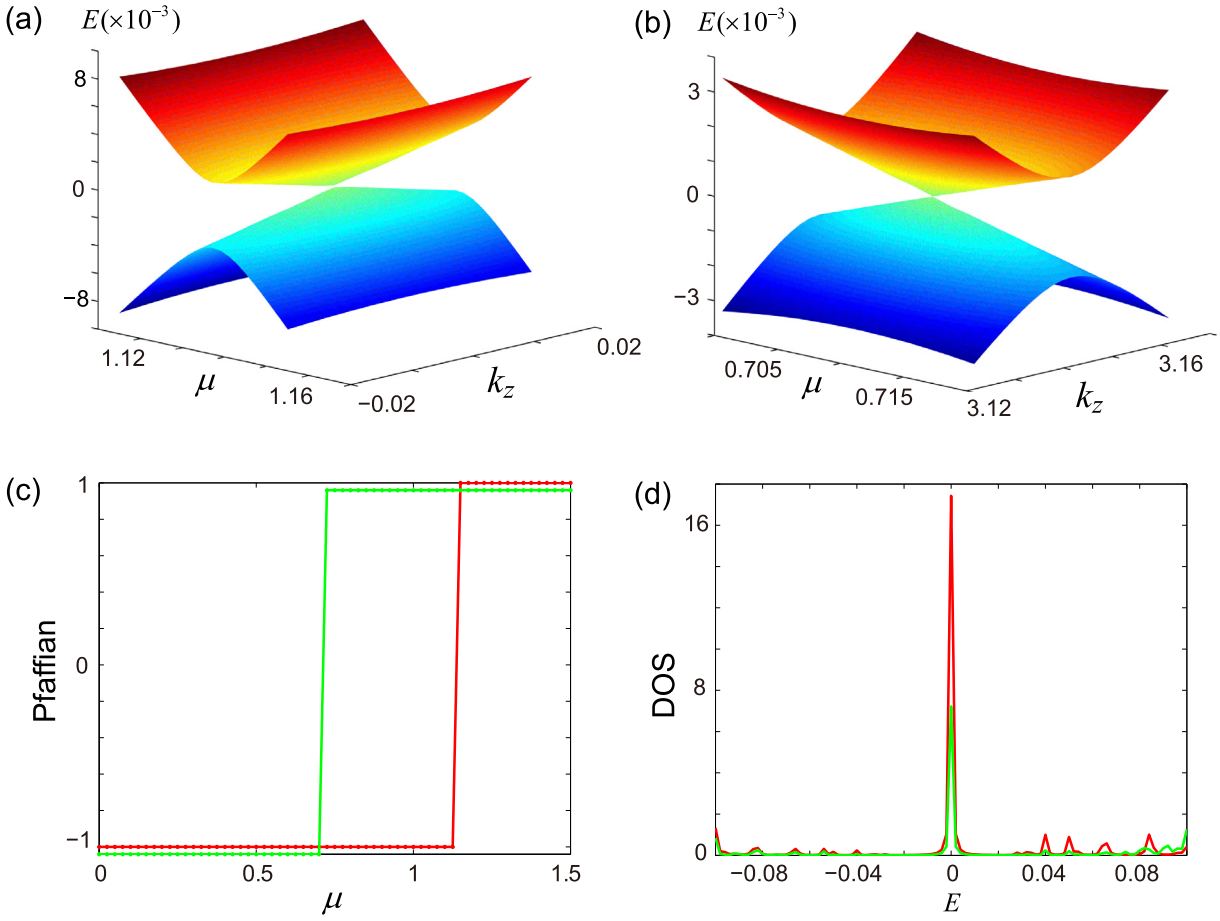

Fig. 1. (Color online) Results of a quantum vortex line in the superconducting state of the WTI in $H_0^{(1)}$. (a) and (b): lowest energy E of the vortex line as a function of the chemical potential μ near $k_z = 0$ and $k_z = \pi$, respectively (the lattice size in the xy-plane is 24×24). Note that $E = 0$ occurs at some critical values of μ for $k_z = 0$ and π. (c): $\mathrm{sgn}(Pf(k_z = 0))$ (red) and $\mathrm{sgn}(Pf(k_z = \pi))$ (green) as functions of μ (the lattice size in the xy-plane is 16×16). The green line is shifted down by 0.04 for visual purpose. (d) the spin resolved local density of states at $\mu = 1.0$, red for spin-up and green for spin-down, at the vortex core on the (001) surface (the lattice size is $14 \times 14 \times 26$). In the calculations, the parameters are $\{t, t_3, t', t_3'\} = \{1.0, 0.5, 1.0, 1.0\}, m = 1.2, \Delta_0 = 0.2$, and the size of the vortex $R \to 0$.

surfaces in the $k_z = 0/\pi$ plane, are $\pm\pi$. Based on this criterion, we have roughly estimated the topological phase transitions by expanding the Hamiltonian in Eq. (3) in the continuum limit. As expected, there are two VPT points: $\mu_1^c = t'\sqrt{2(2t - m + t_3)/t}$ at $k_z = 0$ and $\mu_2^c = t'\sqrt{2(2t - m - t_3)/t}$ at $k_z = \pi$. Apparently, the range of the topologically nontrivial phase is proportional to t_3, namely the coupling strength along the weak coupling direction. It should be emphasized that, if the condition of the superconductivity and the Fermi surfaces are complicated, the Berry phase criterion in Ref. [43] fails to determine the VPT points and we need to calculate the energy spectrum or the Z_2 topological invariant of the vortex line to obtain the VPTs [17,21,44].

From the above analysis, we can achieve topologically nontrivial full-gap vortex line phase in the superconducting WTIs. However, do all the WTIs have similar results? The answer is negative. In fact, the system may not be full-gap [44]. In the following, we show that there is a class of WTIs whose superconducting state with a single quantum vortex line has a robust nodal superconductor phase, rather than a topologically nontrivial full-gap phase. To be specific, we consider the following lattice model

$$\begin{aligned} H_0^{(2)} = {} & (m - t\cos k_x - t\cos k_y - t_3\cos k_z)\Sigma_{30} + t'\sin k_x\Sigma_{13} \\ & + t_3'\sin k_z(\cos k_x - \cos k_y)\Sigma_{11} - t'\sin k_y\Sigma_{20} \\ & + 2t_3'\sin k_z\sin k_x\sin k_y\Sigma_{12}. \end{aligned} \tag{4}$$

Here, $H_0^{(2)}$ respects the same symmetries as $H_0^{(1)}$ in Eq. (3), and the only difference between them is that, one of the Kramers' doublets in the basis is changed into one with the same parity but a different angular momentum quantum number, $\pm\frac{3}{2}$. Correspondingly, the matrix form of the symmetry group generators transforms into $C_{4z} = (\Sigma_{30} + i\Sigma_{03})/\sqrt{2}$ and $C_{2x} = \Sigma_{31}$, while both the inversion symmetry and TRS remain unchanged. We take all the parameters in $H_0^{(2)}$ the same as those in $H_0^{(1)}$, which leads to that the two Hamiltonians have similar topological property.

However, as we shall show below, the topological property of the vortex line in the superconducting state of $H_0^{(2)}$ is completely different from that in $H_0^{(1)}$. In addition to the topological VPTs at $k_z = 0$ and $k_z = \pi$, which occur at exactly the same critical chemical potential μ_1^c and μ_2^c as in the case of $H_0^{(1)}$, for any given k_z, there is also a chemical potential μ so that the vortex line in the superconducting WTIs described by $H_0^{(2)}$ becomes gapless. In Fig. 2a, we show this explicitly for $\mu = 1.0$. Obviously, the vortex line has two nodes at $\pm 0.75\pi$. Moreover, the nodes in the vortex line are rather stable: the nodal points can never be gapped out unless two points meet with each other. In the limit $t_3' = 0$, we can get the trajectory of the nodal points in the (k_z, μ) space. We begin with an infinite large chemical potential μ. As it decreases, a nodal point first emerges at $k_z = 0$ when $\mu = \mu_1^c$. Then the nodal point splits into two and they move in the opposite directions on the k_z-axis. Finally the two nodal points meet with each other at $k_z = \pi$ when $\mu = \mu_2^c$ and gap out. A finite t_3' only changes the condition quantitatively where the nodal points emerge and vanish. Therefore, this is a robust 1D nodal superconducting

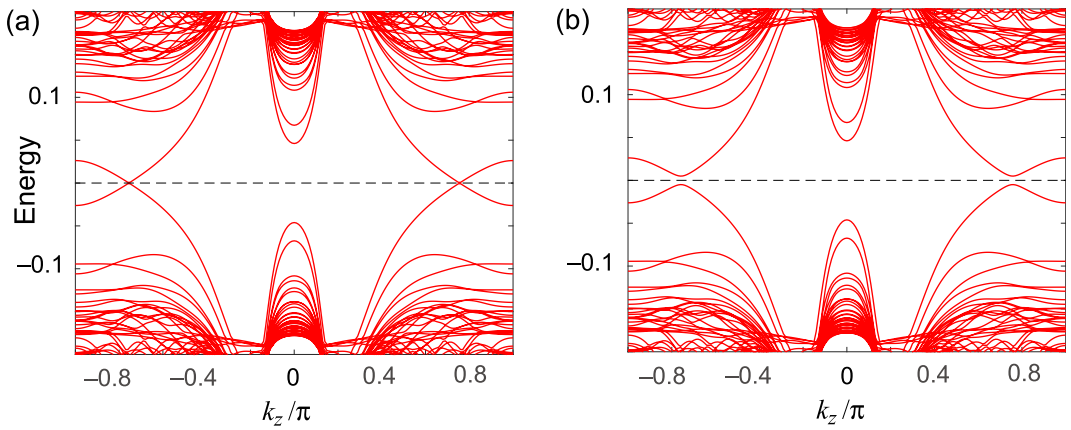

Fig. 2. (Color online) Dispersion of the low-energy bands of the vortex line in a superconducting WTI as a function of k_z for the chemical potential $\mu = 1.0$. (a) The WTI is depicted by $H_0^{(2)}$. Note that there are two nodes at $k_z = \pm 0.75\pi$. (b) The WTI is described by $H_0^{(2)}$ with an additional C_{4z} rotational symmetry breaking term $t_{sb} \sin k_z \Sigma_{11}$, where $t_{sb} = 0.1$. Obviously, the vortex line becomes fully gapped. In the calculations, all other parameters are the same as in Fig. 1.

phase with bulk MZMs [44]. The bulk MZMs behave like the helical Majorana modes [60] protected by the TRS and propagate along the vortex line in the real space. Actually, this nodal phase stems from the fact that, there is a band inversion at every k_z on the Γ-Z line for $H_0^{(2)}$ while it is true only at the Γ point and Z point for $H_0^{(1)}$. If a C_{4z} rotational symmetry broken perturbation $t_{sb} \sin k_z \Sigma_{11}$ is added, $H_0^{(2)}$ still describes a WTI with band inversions at the Γ point and Z point. However, the band inversion on the Γ-Z line ($k_z \neq 0, \pi$) is no longer true. Namely the system is similar to that in $H_0^{(1)}$. Consequently, the energy spectrum of the corresponding vortex line system becomes fully gapped, shown in Fig. 2b.

From the above results, we can find that the WTIs can be classified into two classes according to the topological property of their superconducting vortex line. The WTIs described by $H_0^{(1)}$ and $H_0^{(2)}$ can be viewed as the generalization of the 3D STIs and TDSs respectively. To be specific, the two Hamiltonians both describe 2D TIs if we omit the coupling in the z-direction. With the coupling terms in the z-direction turned on, especially the t_3 term, both of the two Hamiltonians describe 3D WTIs with band inversions at the Γ point and Z point when t_3 is small. As t_3 becomes larger, the WTIs have larger band dispersion in the k_z-direction and the insulating gap closes at the Z point at some critical $t_3 = t^c$. Finally, the WTIs in $H_0^{(1)}$ and $H_0^{(2)}$ evolve into STIs and TDSs with a band inversion at the Γ point respectively with t_3 tuned to be larger. As a result, it can be inferred that the superconducting vortex line for the WTIs in $H_0^{(1)}$ and $H_0^{(2)}$ must have similar topological properties with the STI [43] and TDS [44] case respectively. Recalling the condition for the existence of TDSs [61], we can straightforwardly conclude that the nodal superconducting vortex line phase is stable only when the band inversions of the WTI occur between two bands with nonequivalent angular momentum quantum numbers defined by the C_n ($n > 2$) rotational axis, and in the other case the superconducting WTI plus a single quantum vortex line is full-gap with a single vortex end MZM for certain range of doping level.

3. Generalization to Z_2 trivial insulators with double-band inversions

Based on the above analysis and our previous work in Ref. [44], the topologically nontrivial vortex line state is closely related to the topological property of the normal state, which is determined by the band inversions in the Brillouin zone. In the 3DWTI case, there are two band inversions which occur at different k-points in the Brillouin zone. However, there is another possibility that the two band inversions occur at the same k-point in the Brillouin zone, the so-called double-band inversion. In the normal state, such a double-band inversion can not change the Z_2 topological invariant of the system. However, it can lead to some topologically nontrivial crystalline state, such as the topological mirror insulator state in the antiperovskites A_3SnO [62,63] and wallpaper fermion state in Sr_2Pb_3 [64]. Therefore, it is natural to ask whether the topologically nontrivial vortex line state can be realized in systems with double-band inversion. To illustrate this, we introduce the following model

$$
\begin{aligned}
H_0^{DB} &= \begin{pmatrix} H_{01} & H_{hy} \\ H_{hy}^\dagger & H_{02} \end{pmatrix}, \\
H_{01} &= m_1(k)\Sigma_{30} + v_1[\sin k_x \Sigma_{13} + \sin k_y \Sigma_{20}], \\
H_{02} &= m_2(k)\Sigma_{30} + v_2[\sin k_x \Sigma_{20} - \sin k_y \Sigma_{13}], \\
H_{hy} &= \lambda(\mathrm{i}\sigma_x\tau_+ + \mathrm{i}\sigma_y\tau_-),
\end{aligned}
\tag{5}
$$

where $m_i(k) = M_i - B_i(\cos k_x + \cos k_y)$ $(i = 1, 2)$, $\tau_\pm = \tau_x \pm \mathrm{i}\tau_y$, and the parameters are set to be $\{v_1, v_2, M_1, M_2, B_1, B_2\} = \{0.5, 1.0, 1.5, 1.5, 1.0, 1.0\}$. The above Hamiltonian can be regarded as two copies of 2D TIs when $\lambda = 0$, and H_{hy} is the hybridization between the two TIs respecting both the TRS and inversion symmetry. The TRS and inversion symmetry operators take the matrix form $T = K\mathrm{i}\Sigma_{02}\gamma'_0$ and $I = \Sigma_{30}\gamma_3$ respectively, where γ_i $(i = 1, 2, 3)$ are the Pauli matrices defined in the space constructed by H_{01} and H_{02}. Obviously, when $\lambda = 0$, there will be two Dirac cones on the edge, as shown in Fig. 3a. When H_{hy} is turned on, the two TIs hybridize and the Dirac cones on the edge hybridize as well to open a gap, shown in Fig. 3b, c. Therefore, H_0^{DB} remains topologically trivial for any λ value.

Considering an on-site intra-orbital pairing, we analyze its topological VPTs. As mentioned above, H_0^{DB} can be viewed as two independent 2D TIs when λ is zero. Each of the two superconducting 2D TIs plus a single quantum vortex must go through a VPT at some critical chemical potential μ^c [44]. As a result, if the two TIs have different μ^c, for example μ_1^c (μ_2^c) for H_{01} (H_{02}), the superconducting vortex becomes topologically nontrivial when the chemical potential is between μ_1^c and μ_2^c. With the parameters above, μ_1^c and μ_2^c are determined to be 0.50 and 0.89, shown in Fig. 3d. When a small λ is turned on, the two TIs hybridize with each other. However, the topologically nontrivial vortex state can not be destroyed immediately as the topological phase is protected by a

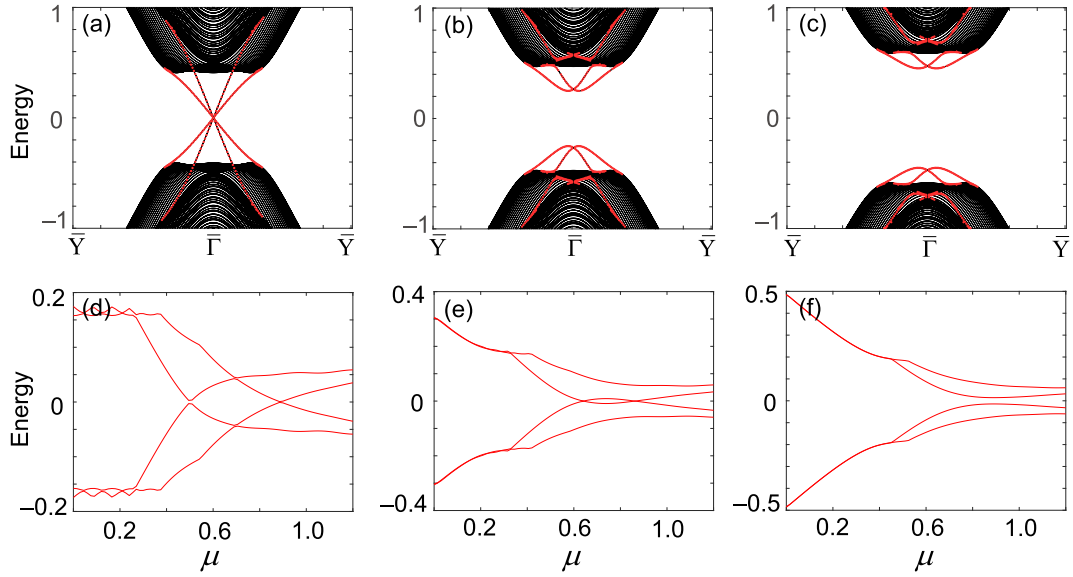

Fig. 3. (Color online) The edge states along the high-symmetry line on the (100) edge for H_0^{DB} are presented in (a)–(c). (d)–(f) show the lowest energies of the 0D superconducting vortex system corresponding to H_0^{DB} as a function of the chemical potential μ. (a), (d) show the results for the $\lambda = 0$ case, (b), (e) for the $\lambda = 0.14$ case, and (c), (f) for $\lambda = 0.25$. In the calculations, the parameters for the superconductivity are the same as in Fig. 1 with the lattice size 20×20.

finite energy gap. As shown in Fig. 3e, there are still two VPT points at $\mu_1^c = 0.63$ and $\mu_2^c = 0.87$ when $\lambda = 0.14$. The topologically nontrivial vortex line phase becomes smaller when the hybridization becomes strong. Eventually, it becomes topologically trivial if the λ is strong enough, as shown in Fig. 3f.

Taking the coupling in the z-direction into consideration, we can summarize the topological VPTs for the STIs, TDSs and WTIs in a general phase diagram shown in Fig. 4a. Specifically, adding $t_3 \cos k_z$ into $m_i(k)$, we can achieve a topological phase diagram for the superconducting vortex line for the systems with double-band inversions similar to that in H_0^{DB}, shown in Fig. 4b. As analyzed above, there are two VPTs at μ_1^c and μ_2^c at $k_z = 0$ resulting from the double-band inversion at the Γ point. In the limit $t_3 = 0$, a same double-band inversion occurs at the Z point, leading to two VPTs at $\mu_3^c = \mu_1^c$ and $\mu_4^c = \mu_2^c$ at $k_z = \pi$. The superconducting vortex line is always topologically trivial. As a small t_3 is turned on, the VPTs at $k_z = \pi$ and $k_z = 0$ take place at different chemical potential values. Consequently, there will be two narrow topologically nontrivial phases when $\mu_3^c < \mu < \mu_1^c$ and $\mu_4^c < \mu < \mu_2^c$ in the electron-dope region, as the $P1$ phase shown in Fig. 4b. The region of the phase is proportional to strength of t_3. If t_3 is tuned to be larger, μ_4^c becomes smaller than μ_1^c and the superconducting vortex line will be topologically nontrivial when $\mu_3^c < \mu < \mu_4^c$ and $\mu_1^c < \mu < \mu_2^c$, which is the $P2$ phase shown in Fig. 4b. When t_3 is large enough ($t_3 > t_c^2$), the double-band inversion at the Z point vanishes, namely there is no VPT at $k_z = \pi$ and the superconducting vortex line is topologically trivial only when $\mu_1^c < \mu < \mu_2^c$. Remarkably, the above topologically nontrivial superconducting vortex line is full-gap when and only when H_{01} and H_{02} in H_0^{DB} both describe STIs or WTIs similar to that in $H_0^{(1)}$, and there can be vortex end MZMs for a certain range of doping level in this case. If at least one of the H_{01} and H_{02} describe WTIs similar to that in $H_0^{(2)}$, the system has a 1D robust nodal superconducting phase.

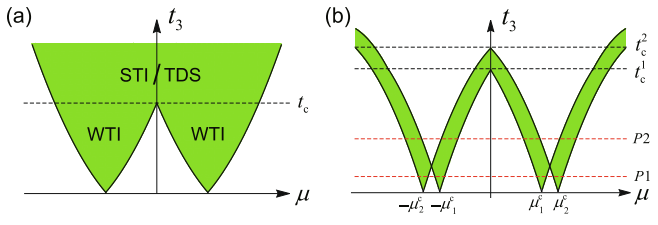

Fig. 4. (Color online) Illustrative topological phase diagrams of the superconducting vortex line as a function of t_3 and the chemical potential μ for the 3D WTIs in Eqs. (3) and (4) in (a) and for the normal insulators with double-band inversion in Eq. (5) in (b). The green region represents the full-gap topologically nontrivial vortex line phase or the quasi-1D nodal superconducting phase, depending on the basis and the symmetry group of the system.

4. Topological VPTs in iron-based SCs

Now we apply the above theory to iron-based SCs. We first focus on the band inversion at the zone center. We take LiOHFeSe as an example, and calculate its band structure with the experimental lattice parameters for $(Li_{0.8}Fe_{0.2})$OHFeSe [65], which is shown in Fig. 5. Without spin-orbital coupling (SOC), there are three major bands near the Γ point, which are labeled as the A_{2u} band and the two-fold degenerate E_g bands, shown in Fig. 5a. With SOC, the E_g bands split into a E_g^+ band and a E_g^- band, as shown in Fig. 5b. The band inversions between the A_{2u} and $E_g^{\pm}$ bands can create nontrivial topological properties as they have opposite parities [66]. In the tetragonal lattice structure in which the C_4 symmetry is preserved, the angular momentum quantum numbers for these bands are $\pm 3/2$ for E_g^+, $\pm 1/2$ for E_g^- and $\pm 1/2$ for A_{2u}. Thus, we can directly apply the above theory to obtain the topological vortex phases caused by the band inversion at Γ point.

The above electronic band structure is qualitively common acrossing all families of iron-based SCs. There are only quantitative differences between different SCs. The major quantiative parameters that can affect the topological properties include the interlayer coupling along c-axis, the relative on-site energy difference between the A_{2u} and E_g bands, the SOC strength and the chemical potential (Fermi energy or carrier density). Depending on these four energy scales, we sketch three typical band structures in Fig. 6a–c for iron-based SCs. Fig. 6a represents a trival phase without a band inversion at high symmetry points. In Fig. 6b, the band inversion between A_{2u} and E_g bands takes place at Z point but not at Γ point. In this case, it represents a 3D STI phase or a TDS phase depending on the chemical potential. If the Fermi energy is set in

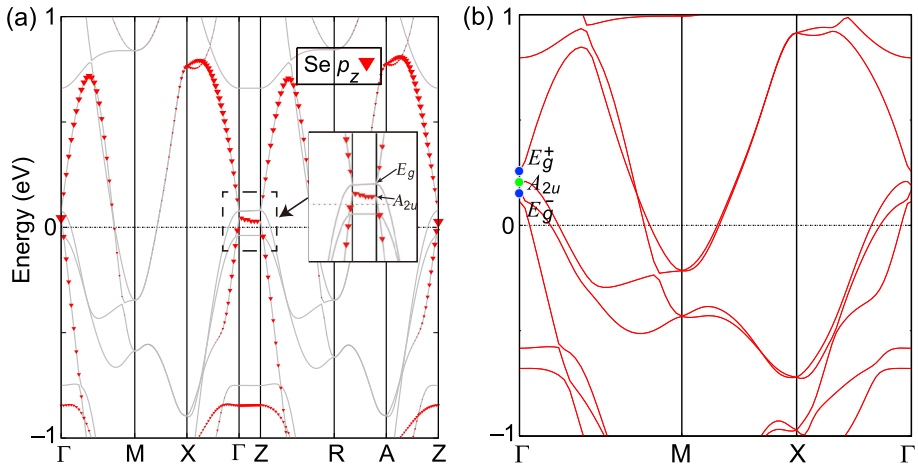

Fig. 5. (Color online) The band structures for LiOHFeSe without SOC (a) and with SOC (b). The bands at Γ point which belong to the E_g (A_{2u}) irreducible representation are marked by the blue (green) point.

between the E_g^- and $A_{2u}(E_g^+)$ bands at the Z point, it is STI (TDS). The topological vortex phases in this region are sketched in Fig. 6d. There are two phases, the topological nodal vortex line (TNVL) phase and topological full-gap vortex line (TFVL) phase with vortex end MZMs, which result from TDS and STI states respectively. A nematic order, which breaks the C_4 rotation symmetry, can drive VPT from the TNVL phase to TFVL phase as shown in Fig. 6d.

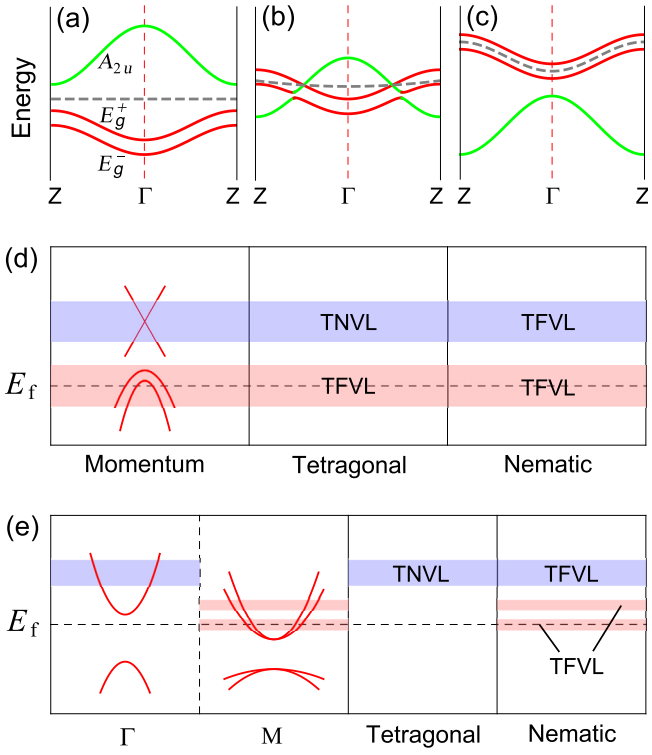

Fig. 6. (Color online) Sketch of the band structures along the Γ-Z line in the Brillouin zone for typical iron-based superconductors and topological phases. (a) Topological trivial band structure; (b) Strong TI or Dirac Semimetal phases; (c) 3D Weak TI case; (d) Topological vortex phases for the (b) case; (e) Topological vortex phases for the (c) case. The case corresponding to the double-band inversion at the Brillouin zone corner M point is also presented in (e). (d) and (e) show the typical band structures of iron-based SCs (left panel) near the high symmetry point in the Brillouin zone, and the regions of the chemical potential (represented by different colors) corresponding to the possible topologically nontrivial vortex line phases in the tetragonal phase (middle panel) and the nematic phase (right panel) of iron-based SCs.

In Fig. 6c, the band inversion between the A_{2u} and E_g bands takes place at both Γ and Z points, which is corresponding to a 3DWTI phase. In this case, the band structure and the topological vortex line phases are sketched in Fig. 6e. In fact, the band of LiOHFeSe shown in Fig. 5 belongs to this case, in which the E_g^+ band and the A_{2u} band have a band inversion at both Γ and Z point. The band inversion is mainly caused by the strong coupling between the Fe-d_{xy} orbital and the Se-p_z orbital in the FeSe layer. The band inversion is known to take place much easylier in a material with a smaller in-plane lattice parameter. As pointed out in Ref. [52], the band inversion occurs when the in-plane lattice parameter is smaller than 3.905 Å. This is consistent with the Li(OH)FeSe case, whose in-plane lattice parameter is only 3.7787 Å [65]. Furthermore, the bands of Li(OH)FeSe disperse weakly along the k_z-direction and there is the band inversion at the Z point as well. Namely, Li(OH)FeSe is a 3D WTI. Furthermore, the E_g^+ band has angular momentum $\pm\frac{3}{2}$ and the A_{2u} band has angular momentum $\pm\frac{1}{2}$ so that the WTI phase of Li(OH)FeSe is of the case described by Eq. (4). As a result, Li(OH)FeSe can only have a narrow nodal superconducting vortex line phase. If there is a nematic order [67–70], as shown in Fig. 6e, the nodal phase can be broken into a full-gap one and vortex end MZMs can emerge on the (001) surface.

Besides the above WTI phase, Ref. [50] points out that a 2D "WTI" state, which is attributed to a double-band inversion at the M point, may exist in single-layer FeSe. For the large lattice parameter in the c-direction, the band structures of LiOHFeSe are similar to that of the single-layer FeSe. Therefore, we also consider the 2D "WTI" phase here. Based on the symmetry analysis, the bands near the Fermi level at the M point in iron-based SCs are described by the following Hamiltonian in the one-Fe unit cell [71]

$$H_0^{\text{iron}} = \begin{pmatrix} H_X & H_{\text{inter}} \\ H_{\text{inter}}^\dagger & H_Y \end{pmatrix}, \tag{6}$$

in which H_X and H_Y describe the bands at the X and Y point (defined in the one-Fe unit cell) respectively, and H_{inter} is the inter-pocket hybridization term. The 2D "WTI" phase in Ref. [50] corresponds to such a condition that, H_{inter} vanishes and both H_X and H_Y describes 2D TIs, which is similar to the system in Eq. (5). However, H_X and H_Y are related with each other by the C_{4z} rotational symmetry in iron-based SCs. That is to say, H_X and H_Y must have the same critical chemical potential, namely $\mu_1^c = \mu_2^c$, resulting in that the 2D "WTI" phase itself can not lead to topologically nontrivial vortex line states. However, it has been intensively studied that the C_{4z} rotational symmetry are intended to be broken, namely, there can

be a nematic order Δ_{ne} [67–70] in doped LiOHFeSe, $(Li_{1-x}Fe_x)$OHFeSe. In this case, the critical chemical potentials for H_X and H_Y are different and satisfy $|\mu_1^c - \mu_2^c| \propto \Delta_{ne}$. When the nematic order is larger than the inter-pocket hybridization, $(Li_{1-x}Fe_x)$OHFeSe must have a topologically nontrivial vortex line phase for certain range of doping level. Furthermore, the above topological phase must be a full-gap one, since the system only has C_{2z} rotational symmetry, which means that there can be vortex end MZMs in $(Li_{1-x}Fe_x)$OHFeSe, as shown in Fig. 6e.

We can extend the above study to other iron-based SCs. Recent studies have shown that there is a TDS phase in LiFeAs [54], $BaFe_2As_2$ [54] and $FeSe_{0.5}Te_{0.5}$ [51] with heavy electron doping. In $LiFe_{0.97}Co_{0.09}As$, the Dirac point about 20 meV above the Fermi level has been observed experimentally [54]. The two Dirac points on the Γ-Z line in LiFeAs are contributed by the band cross between the d_{xz}/d_{yz} and p_z orbitals, whose z-component of the angular momentum are $\pm\frac{3}{2}$ and $\pm\frac{1}{2}$ respectively. Consequently, its superconducting vortex line must be nodal if the chemical potential is near the Dirac points. Besides the TDS phase, LiFeAs also has a STI phase near the Fermi level [54]. Correspondingly, it must has a topologically nontrivial full-gap vortex line phase when it is in the STI phase. Based on the above results, the topological phase diagram for superconducting LiFeAs plus a quantum vortex line should be described by Fig. 6d. Since $FeSe_{0.5}Te_{0.5}$ has similar normal state topological properties with LiFeAs [51,54], its superconducting vortex line has a similar phase diagram.

For the doped LiOHFeSe, $(Li_{1-x}Fe_x)$OHFeSe, besides our above discussion, we also find that the interlayer coupling for the A_{2u} band increases as x increases. Therefore, in principle, there is a critical value, $x = x_c$, at which a topological phase transition from 3DWTI to 3DTDS can take place.

5. Discussion and conclusion

In summary, we study the topological VPTs in iron-based SCs. Besides the previously known phases, we show that there are topological vortex phases associated with the existence of 3DWTI. The phases can be classified into two classes: if the band inversions occur on a C_n $(n > 2)$ rotational axis, and the angular momentums of the orbitals contributing to the band inversions are not equivalent, the superconducting WTI plus a quantum vortex line has a robust 1D nodal superconducting phase with bulk MZMs; otherwise, the superconducting vortex line is full-gap and there can be vortex end MZMs for certain range of doping level. In both cases, the range of the topologically nontrivial phase is proportional to the band dispersion along the weak coupling direction. All these phases can be realized in different families of iron-based SCs by carrier doping and modifying interlayer couplings.

It should be emphasized that, the nodal superconducting vortex line state can only be distinguished from the full-gap one at rather low temperature, since the Caroli-de Gennes-Matricon excitations in a vortex line generally has a tiny gap proportional to Δ^2/E_f [72], where Δ is the superconducting order parameter and E_f is the Fermi energy. For instance, LiFeAs has a T_c about 18 K. If we ignore its topological nontrivial property in normal state, this leads to a full-gap superconducting vortex line with a gap about 0.1 meV when $E_f = 20$ meV. Thus, the temperature to detect the nodal superconducting state must be less than 1 K.

From our study, it is clear that the VPTs are sensitive to the chemical potential in superconducting 3D STI and is even more sensitive in a superconducting 3DWTI. This sensitivity suggests that the disorder can have a strong effect on the VPT. Furthermore, as iron-based SCs are layered structures, the interlayer coupling is weak in general. Considering that the bands in iron-based SCs are known to be renormalized by electron-electron correlations strongly, we can argue that even FeSe/Te can be close to a 3DWTI. This may explain why MZMs only appear in some vortices [38,53].

Conflict of interest

The authors decalre that they have no conflict of interest.

Acknowledgments

This work was supported by the National Basic Research Program of China (2014CB921203, 2015CB921300, and 2017YFA0303100), the National Natural Science Foundation of China (11334012 and 11674278), and the Strategic Priority Research Program of CAS (XDB07000000). S. S. Qin thanks N. N. Hao for helpful discussion.

Author contributions

J. P. Hu and F.-C. Zhang conceived the project. X. X. Wu and X. Dai calculated the band structures and analyzed the topological properties of iron based superconductors. S. S. Qin, L. H. Hu and C. Fang performed numerical simulations and theoretical analysis on the topological properties of the vortex bound states. S. S. Qin, F.-C. Zhang and J. P. Hu wrote the manuscript with inputs from all coauthors.

References

[1] Nayak C, Simon SH, Stern A, et al. Non-Abelian anyons and topological quantum computation. Rev Mod Phys 2008;80:1083.
[2] Chiu CK, Teo JCY, Schnyder AP, et al. Classification of topological quantum matter with symmetries. Rev Mod Phys 2016;88:035005.
[3] Alicea J. New directions in the pursuit of Majorana fermions in solid state systems. Rep Prog Phys 2012;75:076501.
[4] Qi XL, Zhang SC. Topological insulators and superconductors. Rev Mod Phys 2011;83:1057.
[5] Hasan MZ, Kane CL. Colloquium: topological insulators. Rev Mod Phys 2010;82:3045.
[6] Schnyder AP, Ryu S, Furusaki A, et al. Classification of topological insulators and superconductors in three spatial dimensions. Phys Rev B 2008;78:195125.
[7] Ryu S, Schnyder AP, Furusaki A, et al. Topological insulators and superconductors: tenfold way and dimensional hierarchy. New J Phys 2010;12:065010.
[8] Kitaev AY. Unpaired Majorana fermions in quantum wires. Phys Usp 2001;44:131.
[9] Fu L, Kane CL. Superconducting proximity effect and Majorana fermions at the surface of a topological insulator. Phys Rev Lett 2008;100:096407.
[10] Fu L, Berg E. Odd-parity topological superconductors: theory and application to $Cu_xBi_2Se_3$. Phys Rev Lett 2010;105:097001.
[11] Qi XL, Hughes TL, Zhang SC. Chiral topological superconductor from the quantum Hall state. Phys Rev B 2010;82:184516.
[12] Lutchyn RM, Sau JD, Das Sarma S. Majorana fermions and a topological phase transition in semiconductor-superconductor heterostructures. Phys Rev Lett 2010;105:077001.
[13] Oreg Y, Refael G, von Oppen F. Helical liquids and Majorana bound states in quantum wires. Phys Rev Lett 2010;105:177002.
[14] Alicea J, Oreg Y, Refael G, et al. Non-Abelian statistics and topological quantum information processing in 1D wire networks. Nat Phys 2011;7:412.
[15] Sau JD, Lutchyn RM, Tewari S, et al. Generic new platform for topological quantum computation using semiconductor heterostructures. Phys Rev Lett 2010;104:040502.
[16] Chiu CK, Gilbert MJ, Hughes TL. Vortex lines in topological insulator-superconductor heterostructures. Phys Rev B 2011;84:144507.
[17] Chiu CK, Ghaemi P, Hughes TL. Stabilization of Majorana modes in magnetic vortices in the superconducting phase of topological insulators using topologically trivial bands. Phys Rev Lett 2012;109:237009.
[18] Nadj-Perge S, Drozdov IK, Bernevig BA, et al. Proposal for realizing Majorana fermions in chains of magnetic atoms on a superconductor. Phys Rev B 2013;88:020407(R).
[19] Nakosai S, Tanaka Y, Nagaosa N. Topological superconductivity in bilayer Rashba system. Phys Rev Lett 2012;108:147003.
[20] Yang W, Li Y, Wu CJ. Topological septet pairing with spin-$\frac{3}{2}$ fermions: high-partial-wave channel counterpart of the ^{3}He-B phase. Phys Rev Lett 2016;117:075301.
[21] Xu G, Lian B, Tang PZ, et al. Topological superconductivity on the surface of Fe-based superconductors. Phys Rev Lett 2016;117:047001.

[22] Yang G, Stano P, Klinovaja J, et al. Majorana bound states in magnetic skyrmions. Phys Rev B 2016;93:224505.
[23] Chan C, Zhang L, Poon TFJ, et al. Generic theory for Majorana zero modes in 2D superconductors. Phys Rev Lett 2017;119:047001.
[24] Chan C, Liu XJ. Non-Abelian Majorana modes protected by an emergent second Chern number. Phys Rev Lett 2017;118:207002.
[25] Yan ZB, Bi R, Wang Z. Majorana zero modes protected by a Hopf invariant in topologically trivial superconductors. Phys Rev Lett 2017;118:147003.
[26] Zhang R-X, Liu C-X. Crystalline symmetry-protected Majorana mode in number-conserving Dirac semimetal nanowires. Phys Rev Lett 2018;120:156802.
[27] Nishida Y. Is a color superconductor topological? Phys Rev D 2010;81:074004.
[28] Roy B, Goswami P. Z_2 index for gapless fermionic modes in the vortex core of three-dimensional paired Dirac fermions. Phys Rev B 2014;89:144507.
[29] Sasaki S, Kriener M, Segawa K, et al. Topological superconductivity in $Cu_xBi_2Se_3$. Phys Rev Lett 2011;107:217001.
[30] Sun HH, Zhang KW, Hu LH, et al. Majorana zero mode detected with spin selective Andreev reflection in the vortex of a topological superconductor. Phys Rev Lett 2016;116:257003.
[31] Mourik V, Zuo K, Frolov SM, et al. Signatures of Majorana fermions in hybrid superconductor-semiconductor nanowire devices. Science 2012;336:1003.
[32] Das A, Ronen Y, Most Y, et al. Zero-bias peaks and splitting in an Al-CInAs nanowire topological superconductor as a signature of Majorana fermions. Nat Phys 2012;8:887.
[33] Deng MT, Yu CL, Huang GY, et al. Anomalous zero-bias conductance peak in a Nb-CInSb nanowire-CNb hybrid device. Nano Lett 2012;12:6414.
[34] Rokhinson LP, Liu X, Furdyna JK. The fractional a.c. Josephson effect in a semiconductor-superconductor nanowire as a signature of Majorana particles. Nat Phys 2012;8:795.
[35] Perge SN, Drozdov IK, Li J, et al. Observation of Majorana fermions in ferromagnetic atomic chains on a superconductor. Science 2014;346:602.
[36] He QL, Pan L, Stern AL, et al. Chiral Majorana fermion modes in a quantum anomalous Hall insulator-superconductor structure. Science 2017;357:294–9.
[37] Wang DF, Kong LY, Fan P, et al. Evidence for Majorana bound state in an iron-based superconductor. arXiv:1706.06074, 2017.
[38] Zhang P, Yaji K, Hashimoto T, et al. Observation of topological superconductivity on the surface of an iron-based superconductor. Science 2018;360:182–6.
[39] Kane CL, Mele EJ. Z_2 topological order and the quantum spin Hall effect. Phys Rev Lett 2005;95:146802.
[40] Kane CL, Mele EJ. Quantum spin Hall effect in graphene. Phys Rev Lett 2005;95:226801.
[41] Kane CL, Mele EJ. A new spin on the insulating state. Science 2006;314:1692–3.
[42] Bernevig BA, Zhang SC. Quantum spin Hall effect. Phys Rev Lett 2006;96:106802.
[43] Hosur P, Ghaemi P, Mong RSK, et al. Majorana modes at the ends of superconductor vortices in doped topological insulators. Phys Rev Lett 2011;107:097001.
[44] Qin SS, Hu LH, Le CC, et al. Quasi-1D topological nodal vortex line phase in doped superconducting 3D Dirac semimetals. Phys Rev Lett 2019;123:027003.
[45] Bansil A, Lin H, Das T. Colloquium: topological band theory. Rev Mod Phys 2016;88:021004.
[46] Young SM, Zaheer S, Teo JCY, et al. Dirac semimetal in three dimensions. Phys Rev Lett 2012;108:140405.
[47] Wang ZJ, Sun Y, Chen XQ, et al. Dirac semimetal and topological phase transitions in A_3Bi (A=Na, K, Rb). Phys Rev B 2012;85:195320.
[48] Wang ZJ, Weng HM, Wu QS, et al. Three-dimensional Dirac semimetal and quantum transport in Cd_3As_2. Phys Rev B 2013;88:125427.
[49] Fu L, Kane CL, Mele EJ. Topological insulators in three dimensions. Phys Rev Lett 2007;98:106803.
[50] Hao NN, Hu JP. Topological phases in the single-layer FeSe. Phys Rev X 2014;4:031053.
[51] Wang ZJ, Zhang P, Xu G, et al. Topological nature of the $FeSe_{0.5}Te_{0.5}$ superconductor. Phys Rev B 2015;92:115119.
[52] Wu XX, Qin SS, Liang Y, et al. Topological characters in $Fe(Te_{1-x}Se_x)$ thin films. Phys Rev B 2016;93:115129.
[53] Liu Q, Chen C, Zhang T, et al. Robust and clean Majorana zero mode in the vortex core of high-temperature superconductor $(Li_{0.84}Fe_{0.16})$OHFeSe. arXiv:1807.01278, 2018.
[54] Zhang P, Wang ZJ, Wu XX, et al. Multiple topological states in iron-based superconductors. arXiv:1809.09977, 2018.
[55] Fang C, Gilbert MJ, Bernevig BA. New class of topological superconductors protected by magnetic group symmetries. Phys Rev Lett 2014;112:106401.
[56] Budich JC, Ardonne E. Equivalent topological invariants for one-dimensional Majorana wires in symmetry class D. Phys Rev B 2013;88:075419.
[57] He JJ, Ng TK, Lee PA, et al. Selective equal-spin Andreev reflections induced by Majorana fermions. Phys Rev Lett 2014;112:037001.
[58] Hu LH, Li C, Xu DH, et al. Theory of spin-selective Andreev reflection in the vortex core of a topological superconductor. Phys Rev B 2016;94:224501.
[59] Jeon S, Xie YL, Li J, et al. Distinguishing a Majorana zero mode using spin-resolved measurements. Science 2017;358:772.
[60] Zhang F, Kane CL, Mele EJ. Time-reversal-invariant topological superconductivity and Majorana Kramers pairs. Phys Rev Lett 2013;111:056402.
[61] Yang BJ, Nagaosa N. Classification of stable three-dimensional Dirac semimetals with nontrivial topology. Nat Commun 2014;5:4898.
[62] Hsieh TH, Liu JW, Fu L. Topological crystalline insulators and Dirac octets in antiperovskites. Phys Rev B 2014;90:081112(R).
[63] Oudah M, Ikeda A, Hausmann JN, et al. Superconductivity in the antiperovskite Dirac-metal oxide $Sr_{3-x}SnO$. Nat Commun 2016;7:13617.
[64] Wieder BJ, Bradlyn B, Wang ZJ, et al. Wallpaper fermions and the nonsymmorphic Dirac insulator. Science 2018;361:246–51.
[65] Lu XF, Wang NZ, Wu H, et al. Coexistence of superconductivity and antiferromagnetism in $(Li_{0.8}Fe_{0.2})$OHFeSe. Nat Mater 2015;14:325–9.
[66] Fu L, Kane CL. Topological insulators with inversion symmetry. Phys Rev B 2007;76:045302.
[67] Mukherjee S, Kreisel A, Hirschfeld PJ, et al. Model of electronic structure and superconductivity in orbitally ordered FeSe. Phys Rev Lett 2015;115:026402.
[68] Watson MD, Kim TK, Haghighirad AA, et al. Emergence of the nematic electronic state in FeSe. Phys Rev B 2015;91:155106.
[69] Zhang P, Qian T, Richard P, et al. Observation of two distinct d_{xz}/d_{yz} band splittings in FeSe. Phys Rev B 2015;91:214503.
[70] Wu XX, Liang Y, Fan H, et al. Nematic orders and nematicity-driven topological phase transition in FeSe. arXiv:1603.02055, 2016.
[71] Cvetkovic V, Vafek O. Space group symmetry, spin-orbit coupling, and the low-energy effective Hamiltonian for iron-based superconductors. Phys Rev B 2013;88:134510.
[72] Caroli C, de Gennes PG, Matricon J. Bound Fermion states on a vortex line in a type II superconductor. Phys Lett 1964;9:307.

Shengshan Qin received his Ph.D. degree from IOP/CAS in 2018. He is currently a postdoctoral fellow in Kavli Institute for Theoretical Sciences. His research mainly centers on the novel topological systems in condensed matter physics, including topological insulators, semimetals, and superconductors.

Fu-Chun Zhang received his college study in Fudan University and Ph.D. degree in Physics at Virginia Tech. USA in 1983. He was a postdoctoral fellow in University of Minnesota, University of Maryland and ETH-Zurich before he took a professorship at the University of Cincinnati, USA in 1988. He then moved to the University of Hong Kong in 2003, where he worked for about 10 years. He has been the director of Kavli Institute for Theoretical Sciences at the University of Chinese Academy of Sciences since 2017 after he served for Zhejiang University for several years as a professor. He is a Fellow of American Physical Society. His research interests are strong correlated electrons and topological states in condensed matter physics.

Jiangping Hu received his Ph.D. degree from Stanford University (2002), was a postdoctoral fellow at UCLA (2002–2004), and was a faculty member at Purdue University (2004–2012). Hu is a Fellow of American Physical Society. Currently, he leads a research group in the Institute of Physics (IOP/CAS), focusing on studying strongly correlated electron systems and topological materials.